



## OPEN ACCESS

## EDITED BY

Tianying Sun,  
Sun Yat-sen University, China

## REVIEWED BY

Yueyue Pan,  
University of Toronto, Canada  
Xian Chen,  
Shenzhen University, China

## \*CORRESPONDENCE

Qu Zhou,  
✉ zhouqu@swu.edu.cn

RECEIVED 11 October 2024

ACCEPTED 18 November 2024

PUBLISHED 27 November 2024

## CITATION

Zhang H, Xu H, Zeng W, Wang Z and Zhou Q (2024) Gas sensing performance of  $Ti_3C_2T_x$  MXene heterojunction structures in greenhouse environments: a mini review. *Front. Chem.* 12:1509732. doi: 10.3389/fchem.2024.1509732

## COPYRIGHT

© 2024 Zhang, Xu, Zeng, Wang and Zhou. This is an open-access article distributed under the terms of the [Creative Commons Attribution License \(CC BY\)](https://creativecommons.org/licenses/by/4.0/). The use, distribution or reproduction in other forums is permitted, provided the original author(s) and the copyright owner(s) are credited and that the original publication in this journal is cited, in accordance with accepted academic practice. No use, distribution or reproduction is permitted which does not comply with these terms.

# Gas sensing performance of $Ti_3C_2T_x$ MXene heterojunction structures in greenhouse environments: a mini review

Haoming Zhang<sup>1</sup>, Hongyu Xu<sup>1</sup>, Wen Zeng<sup>2</sup>, Zhongchang Wang<sup>3</sup> and Qu Zhou<sup>1\*</sup>

<sup>1</sup>College of Engineering and Technology, Southwest University, Chongqing, China, <sup>2</sup>College of Materials Science and Engineering, Chongqing University, Chongqing, China, <sup>3</sup>Department of Quantum and Energy Materials, International Iberian Nanotechnology Laboratory (INL), Braga, Portugal

With the continuous advancement of smart greenhouse technologies, digital and information-based environmental monitoring has emerged as a focal point of research. The development of high-performance gas sensors is central to achieving this objective. In recent years, MXene materials have been widely applied in the field of gas sensors due to their excellent ion mobility, favorable hydrophilicity, outstanding electronic conductivity, and unique physicochemical properties. Various MXene heterojunction structures have been synthesized for gas detection. This review aims to summarize the current state of research on  $Ti_3C_2T_x$ -based gas sensors, explore methods for synthesizing different morphologies of  $Ti_3C_2T_x$  heterojunction structures, and evaluate the sensing behaviors of these configurations to fully harness their potential for gas monitoring in greenhouse environments. Additionally, an in-depth analysis of the sensing mechanisms associated with  $Ti_3C_2T_x$  heterojunction structures will be provided, offering theoretical support for future investigations. The findings indicate that  $Ti_3C_2T_x$ -based nanomaterials demonstrate considerable promise as high-performance sensors for gas detection in greenhouse settings. This innovative research not only provides new insights into the development of gas sensor technologies but also serves as an important foundation for the digitization of environmental monitoring.

## KEYWORDS

$Ti_3C_2T_x$ , heterojunction, gas sensor, greenhouse, sensing mechanism

## 1 Introduction

In recent years, greenhouses have become essential facilities for agricultural production; however, their relatively enclosed environments lead to the accumulation of toxic and harmful gases released from improper fertilizer application and insufficient ventilation (Assimakopoulos et al., 2024; Xu et al., 2024). This phenomenon has exacerbated air quality issues within greenhouses. For instance, when ammonia ( $NH_3$ ) concentration exceeds  $5\text{ mg/m}^3$  (approximately 6.579 ppm), crop leaves may exhibit water-soaked spots, ultimately resulting in wilting; at concentrations above  $30\text{ mg/m}^3$  (approximately 39.474 ppm),  $NH_3$  binds with hemoglobin, causing symptoms such as chest tightness, cough, and respiratory difficulties, alongside conjunctival congestion and headaches (Hassan et al., 2024; Huang W. et al., 2024; Wang X. et al., 2024). Similarly, when

nitrogen dioxide (NO<sub>2</sub>) concentration surpasses 5 mg/m<sup>3</sup> (approximately 2.433 ppm), water-soaked spots appear on the edges of crop leaves, which quickly fade to a bleached appearance; if concentrations exceed 20 mg/m<sup>3</sup> (approximately 9.73 ppm), NO<sub>2</sub> can inhibit enzyme activity in humans, affecting the nervous system and leading to chest tightness and respiratory distress, with long-term exposure potentially resulting in neurosis and chronic respiratory inflammation (Lu D. et al., 2023; Kwon et al., 2024; Zhang et al., 2024a). Furthermore, elevated levels of ethylene (C<sub>2</sub>H<sub>4</sub>), exceeding 2 mg/m<sup>3</sup> (approximately 1.598 ppm), significantly impact the edges of leaves and young shoots, manifesting as chloroplast degradation that leads to yellowing or whitening of the leaves. Although ethylene exhibits low toxicity to humans, prolonged exposure may induce symptoms such as dizziness and lack of concentration; high concentrations can even cause paralysis (Zhang et al., 2020; Walubengo et al., 2022; Kormann et al., 2024). Therefore, the development of high-response and low-detection-limit sensors for real-time monitoring of toxic gases within greenhouse environments at room temperature is of critical significance. Such advancements would not only ensure healthy crop growth but also protect the health of agricultural workers, thereby supporting the progression of smart agriculture. Furthermore, it is essential to recognize that humidity levels within greenhouse settings play a pivotal role in determining sensor performance. Fluctuations in moisture can markedly influence both the sensitivity and stability of gas detection mechanisms, necessitating the design of sensors that can effectively operate under varying humidity conditions. This adaptability is crucial for ensuring accurate and reliable monitoring, as excessive moisture may lead to false readings or degradation of sensor materials. Addressing these challenges will enhance the efficacy of gas sensors in dynamic agricultural environments, ultimately contributing to improved environmental control and optimal crop management practices (Singh et al., 2024; Zhang T. et al., 2024; Zhao H. et al., 2024).

MXenes are a class of two-dimensional (2D) materials that have emerged as popular alternatives to graphene in recent years. Composed of transition metals (Sc, Ti, V, Cr, Zr, Nb, Mo, Hf, and Ta), X (C or N), and surface functional groups T (-O, -OH, and -F), MXenes are represented by the chemical formula M<sub>n+1</sub>X<sub>n</sub>T<sub>x</sub>, where n ranges from 1 to 3 (Li Q. et al., 2021; Xia et al., 2023; Wang Y. et al., 2024). Due to their exceptional ion mobility, favorable hydrophilicity, and outstanding electronic conductivity, MXenes have found extensive applications in sensors, catalysts, lithium-ion batteries, electromagnetic shielding, and supercapacitors (Li et al., 2023; Pang et al., 2023; Chen et al., 2024; Zhang J. et al., 2024). Zhang et al. successfully synthesized accordion-like V<sub>2</sub>CT<sub>x</sub> MXene materials and combined them with SnS<sub>2</sub> nanosheets, resulting in the development of a highly efficient MXene heterojunction gas sensor (Zhang et al., 2024d). Gas sensing results indicate that the V<sub>2</sub>CT<sub>x</sub> material composite with SnS<sub>2</sub> nanosheets exhibits an exceptional sensitivity towards NO<sub>2</sub>, being 581 times greater than that of intrinsic V<sub>2</sub>CT<sub>x</sub> materials. Furthermore, at a relative humidity of 51.9%, rapid response and recovery times of 4.8 s and 4.7 s, respectively, are observed, alongside commendable selectivity. Wang et al. successfully incorporated SnS<sub>2</sub> onto Nb<sub>4</sub>C<sub>3</sub>T<sub>x</sub> materials through an *in situ* growth approach (Wang W. et al., 2024). This composite demonstrates a high response of

1046.6% to 50 ppm triethylamine at room temperature, with a response time of 11 s. Lu et al. designed a MXene/Na<sub>2</sub>Ti<sub>3</sub>O<sub>7</sub>@ polyaniline composite, which exhibits a response of 283% to NH<sub>3</sub> at room temperature with 90% humidity and achieves a detection limit of 186% (Lu et al., 2024). Mo<sub>2</sub>CT<sub>x</sub> nanospheres were synthesized using ultrasonic technology by Wang et al. (Wang B. et al., 2024). Gas sensing tests revealed that this material exhibits a favorable response to 5 ppm of NO<sub>2</sub> at room temperature. Additionally, a sensor composed of Nb<sub>2</sub>CT<sub>x</sub> nanosheets combined with polyaniline was fabricated, demonstrating high selectivity and sensitivity towards low-concentration NH<sub>3</sub> at room temperature and 87.1% relative humidity (Wang et al., 2021). Collectively, the synthesis of MXene heterojunction structures holds promise for achieving outstanding gas sensing capabilities for toxic gases in greenhouse environments at room temperature, thereby providing robust technical support for the advancement of smart agriculture.

Ti<sub>3</sub>C<sub>2</sub>T<sub>x</sub> is among the most stable and cost-effective MXene materials, with a well-established preparation methodology. Its exceptional thermal stability, high electrical conductivity, and outstanding chemical and physical properties position it as a potential candidate for climate monitoring applications (Chen et al., 2021; Li W. et al., 2021; Qi et al., 2021). A two-dimensional α-Fe<sub>2</sub>O<sub>3</sub>/Ti<sub>3</sub>C<sub>2</sub>T<sub>x</sub> MXene composite was designed by Zhang et al. (Zhang D. et al., 2024), and gas sensing tests demonstrated that this material exhibits a response of 0.27–100 ppm H<sub>2</sub>S at room temperature, with an exceptionally low detection limit. A unique sacrificial technique was employed by Qiu et al. to successfully fabricate Pd/Cu-modified Ti<sub>3</sub>C<sub>2</sub>T<sub>x</sub> materials, which demonstrate a response time of 4 s to 0.5% H<sub>2</sub> at room temperature, with a detection limit of 0.1% H<sub>2</sub> (Qiu et al., 2024). Li et al. successfully fabricated Fe<sub>2</sub>O<sub>3</sub>/TiO<sub>2</sub>/Ti<sub>3</sub>C<sub>2</sub>T<sub>x</sub> MXene composite sensors, which respond to 100 ppm NH<sub>3</sub> at room temperature with response and recovery times of 62 s and 74 s, respectively (Li et al., 2024). Additionally, a Google Scholar investigation into the keyword “nano + Ti<sub>3</sub>C<sub>2</sub>T<sub>x</sub> + gas sensor” revealed a steady increase in the publication count related to this topic from 2020 to 2023, with records showing 9, 22, 59, and 64 publications annually. Although this data may not be entirely precise, an increasing body of literature indicates that gas sensors based on Ti<sub>3</sub>C<sub>2</sub>T<sub>x</sub> are garnering heightened attention. Therefore, summarizing the latest advancements in Ti<sub>3</sub>C<sub>2</sub>T<sub>x</sub>-based gas sensors is crucial for a deeper understanding of their advantages in monitoring toxic gases within greenhouse environments. This will not only provide a foundation for future research but also establish robust theoretical support for the development of smart agriculture.

In this review, several highly cited published studies have been selected to provide a concise overview of typical Ti<sub>3</sub>C<sub>2</sub>T<sub>x</sub> MXene gas sensors. The objective of this research is to summarize and compare the exceptional performance characteristics of these gas sensors. Furthermore, various methods for synthesizing Ti<sub>3</sub>C<sub>2</sub>T<sub>x</sub> MXene-based materials are presented to offer valuable references for related investigations. Finally, a brief exploration of the sensing mechanisms associated with Ti<sub>3</sub>C<sub>2</sub>T<sub>x</sub> MXene gas sensors is conducted. This review not only establishes a foundation for understanding the applications of Ti<sub>3</sub>C<sub>2</sub>T<sub>x</sub> MXenes in the realm of gas sensing but also elucidates potential directions for future research.

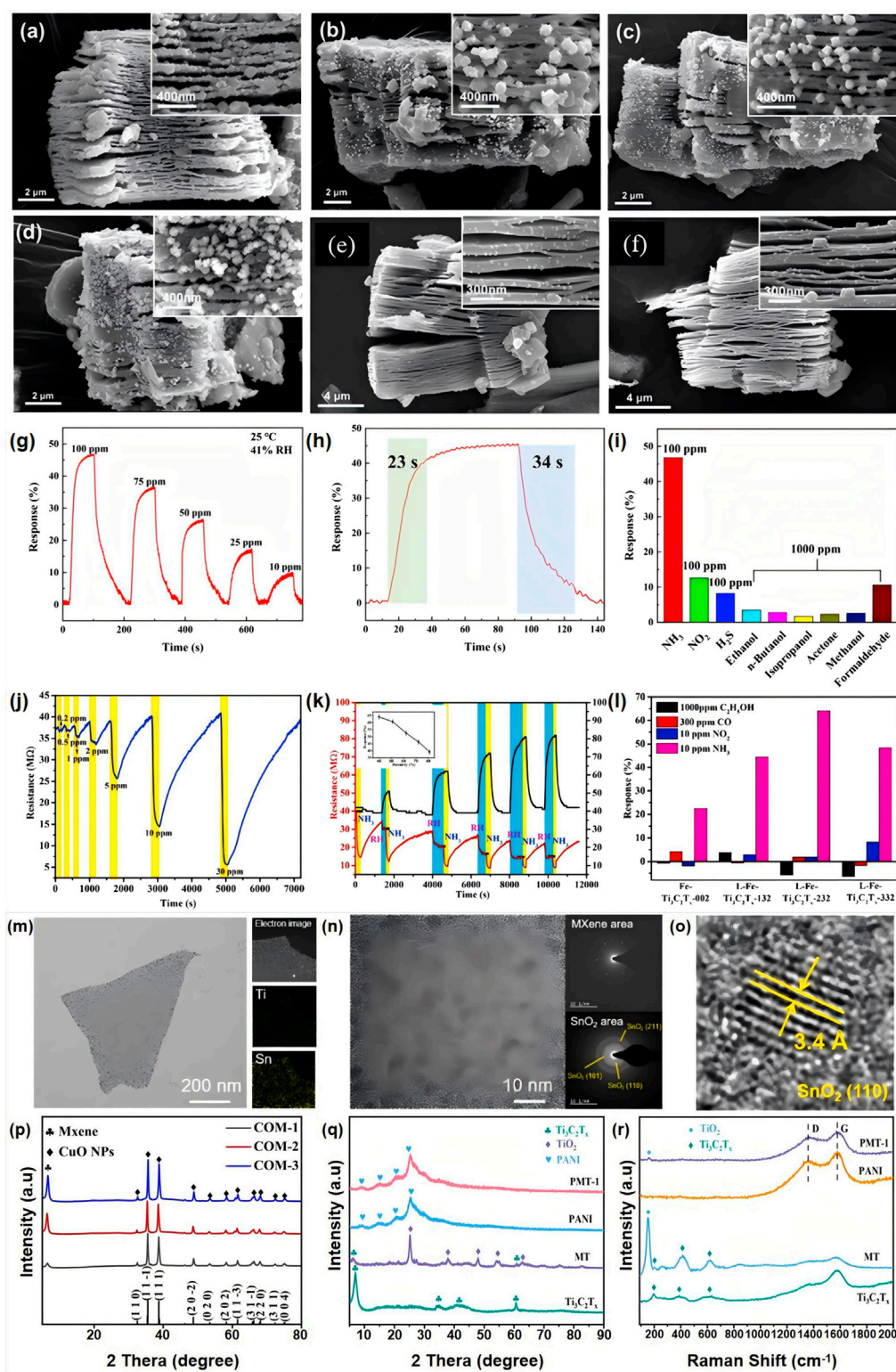


FIGURE 1

Cross-sectional SEM images of (A) Au (0.29 at%) -  $\text{Ti}_3\text{C}_2\text{T}_x$ , (B) Au (1.06 at%) -  $\text{Ti}_3\text{C}_2\text{T}_x$ , (C) Au (1.92 at%) -  $\text{Ti}_3\text{C}_2\text{T}_x$ , (D) Au (2.48 at%) -  $\text{Ti}_3\text{C}_2\text{T}_x$  MXenes, (E) Pt (0.57 at%) -  $\text{Ti}_3\text{C}_2\text{T}_x$ , (F) Pt (0.83 at%) -  $\text{Ti}_3\text{C}_2\text{T}_x$ , reproduced with permission from (Nam et al., 2024). (G) Dynamic response curve of Pt- $\text{Ti}_3\text{C}_2\text{T}_x/\text{TiO}_2$  sensor at room temperature, (H) Typical response/recovery time of Pt- $\text{Ti}_3\text{C}_2\text{T}_x/\text{TiO}_2$  sensor to 100 ppm  $\text{NH}_3$ , (I) Selectivity, reproduced with permission from (Zhang et al., 2023). (J) Response-recovery curve of the L-Fe- $\text{Ti}_3\text{C}_2\text{T}_x$ -232 sensor toward 0.2–30 ppm  $\text{NH}_3$  at RT, (K) Dynamic response-recovery curve of the L-Fe- $\text{Ti}_3\text{C}_2\text{T}_x$ -232 sensor toward 10 ppm  $\text{NH}_3$  at RT along with different RH. The inset displays the plot of the response vs. RH for 10 ppm  $\text{NH}_3$ , (L) Selectivity of the sensors toward 1000 ppm ethanol, 300 ppm CO, 10 ppm  $\text{NO}_2$ , and 10 ppm  $\text{NH}_3$  gas, reproduced with permission from (Qin et al., 2023). (M) TEM image and elemental mapping analysis of a  $\text{SnO}_2$ -MXene hybrid nanosheet. (N) Magnified TEM image of  $\text{SnO}_2$ -MXene hybrid. Insets on the right show Selected Area Electron Diffraction patterns for the exposed MXene area and  $\text{SnO}_2$  area. (O) High-Resolution Transmission Electron Microscopy (HRTEM) image of  $\text{SnO}_2$ -MXene hybrid. (Continued)

## FIGURE 1 (Continued)

Electron Microscopy image of SnO<sub>2</sub> nanoparticle, reproduced with permission from (Yang et al., 2024). (P) XRD spectra of COM-1, COM-2, COM-3 (CuO NPs: MXene = 1:1; CuO NPs: MXene = 1:2; CuO NPs: MXene = 1:3), reproduced with permission from (Peng et al., 2024). (Q) XRD Patterns and (R) Raman spectra of Ti<sub>3</sub>C<sub>2</sub>T<sub>x</sub>, MT, PANI and PMT, reproduced with permission from (Xiong et al., 2023).

## 2 Recent advances in the gas sensing performance of Ti<sub>3</sub>C<sub>2</sub>T<sub>x</sub>

### 2.1 Metal atom modification of Ti<sub>3</sub>C<sub>2</sub>T<sub>x</sub> MXene nanomaterials

Nam et al. successfully developed gas sensors based on Au/Pt-modified Ti<sub>3</sub>C<sub>2</sub>T<sub>x</sub> MXene (Nam et al., 2024). The Ti<sub>3</sub>C<sub>2</sub>T<sub>x</sub> MXene material was synthesized through the HF etching of Ti<sub>3</sub>AlC<sub>2</sub>. The Ti<sub>3</sub>C<sub>2</sub>T<sub>x</sub> MXene materials modified with varying ratios of Au/Pt particles are illustrated in Figures 1A–F. These sensors demonstrated the capability to operate in self-heating mode at room temperature, exhibiting good selectivity towards ammonia when containing 1.92 at% Au or 0.83 at% Pt NPs. Additionally, the Au-Ti<sub>3</sub>C<sub>2</sub>T<sub>x</sub> MXene and Pt-Ti<sub>3</sub>C<sub>2</sub>T<sub>x</sub> MXene sensors demonstrate adaptability to voltages of 5 V and 3 V, respectively, and both have successfully passed rigorous strength tests. These findings indicate that noble metal-modified Ti<sub>3</sub>C<sub>2</sub>T<sub>x</sub> MXene exhibits excellent compatibility for gas detection at room temperature. This research provides novel insights into the development of high-performance gas sensors.

A method for the preparation of Pt-modified Ti<sub>3</sub>C<sub>2</sub>T<sub>x</sub>/TiO<sub>2</sub> heterojunction sensors using a simple hydrothermal approach was proposed by Zhang et al. (Zhang et al., 2023). Experimental comparative results indicate that the response direction of the Pt-modified Ti<sub>3</sub>C<sub>2</sub>T<sub>x</sub>/TiO<sub>2</sub> system changes significantly, enhancing its NH<sub>3</sub> detection performance at room temperature compared to intrinsic Ti<sub>3</sub>C<sub>2</sub>T<sub>x</sub> materials and Ti<sub>3</sub>C<sub>2</sub>T<sub>x</sub>/TiO<sub>2</sub> heterojunctions. As shown in Figure 1G, the response of the Pt-modified Ti<sub>3</sub>C<sub>2</sub>T<sub>x</sub>/TiO<sub>2</sub> heterojunction sensor to 100 ppm NH<sub>3</sub> at room temperature is 45.5%, which is 13.8 times and 10.8 times greater than that of the intrinsic Ti<sub>3</sub>C<sub>2</sub>T<sub>x</sub> material and the Ti<sub>3</sub>C<sub>2</sub>T<sub>x</sub>/TiO<sub>2</sub> heterojunction, respectively. Furthermore, the Pt-modified Ti<sub>3</sub>C<sub>2</sub>T<sub>x</sub>/TiO<sub>2</sub> heterojunction sensor offers advantages such as low detection limits, high response, rapid response and recovery times, and selectivity, as illustrated in Figures 1H, I. In terms of long-term stability and durability under greenhouse conditions, the Pt-Ti<sub>3</sub>C<sub>2</sub>T<sub>x</sub>/TiO<sub>2</sub> sensor exhibited a slight decrease in response to 100 ppm NH<sub>3</sub> after a duration of 22 days. This research provides new insights into the development of efficient gas sensors, particularly for monitoring harmful gases under ambient conditions.

Qin et al. reported an environmentally friendly and efficient one-step pulsed laser ablation method for synthesizing iron cluster-loaded Ti<sub>3</sub>C<sub>2</sub>T<sub>x</sub> MXene (L-Fe-Ti<sub>3</sub>C<sub>2</sub>T<sub>x</sub>) gas sensing materials (Qin et al., 2023). Subsequently, the research team developed sensors based on L-Fe-Ti<sub>3</sub>C<sub>2</sub>T<sub>x</sub> nanosheets to enable real-time detection of NH<sub>3</sub> at room temperature. As illustrated in Figures 1J–L, the L-Fe-Ti<sub>3</sub>C<sub>2</sub>T<sub>x</sub>-232 sensor exhibited a response of 64.03% under 10 ppm NH<sub>3</sub> conditions and demonstrated significant reproducibility even in high-humidity environments, making it a strong candidate for

specific applications such as agricultural monitoring and human health assessment. This exceptional ammonia sensing performance is primarily attributed to the robust adsorption capability conferred by the abundant defect sites on the Ti<sub>3</sub>C<sub>2</sub>T<sub>x</sub> nanosheets, along with the catalytic effects provided by the supported iron clusters. The L-Fe-Ti<sub>3</sub>C<sub>2</sub>T<sub>x</sub>-232 sensor demonstrated commendable long-term stability and durability under greenhouse conditions, maintaining consistent responsiveness to 10 ppm NH<sub>3</sub> over a continuous monitoring period of 44 days. This study introduces a method for modifying Ti<sub>3</sub>C<sub>2</sub>T<sub>x</sub> materials with non-noble metal clusters, thereby further enhancing the sensing performance of Ti<sub>3</sub>C<sub>2</sub>T<sub>x</sub> MXene materials compared to previous research. Such advancements are poised to not only advance gas sensing technology but also open new avenues for practical applications in related fields.

### 2.2 Metal oxide composite Ti<sub>3</sub>C<sub>2</sub>T<sub>x</sub> MXene nanomaterials

Kale et al. developed a Ti<sub>3</sub>C<sub>2</sub>T<sub>x</sub> material with optimized surface terminating groups (-O and -OH), utilizing 30% HF as an etching agent to enhance the interaction with ammonia molecules, designated as Ti<sub>3</sub>C<sub>2</sub>T<sub>x</sub>-30 (Kale et al., 2024). This material exhibits the advantage of a low work function (3.78 eV) and is embedded in a MoO<sub>3</sub> matrix to achieve both high sensitivity and room temperature operation. The MoO<sub>3</sub> matrix provides stability to Ti<sub>3</sub>C<sub>2</sub>T<sub>x</sub>-30, effectively reducing its risk of oxidation, while Ti<sub>3</sub>C<sub>2</sub>T<sub>x</sub>-30 introduces additional free electrons into the MoO<sub>3</sub> matrix, enabling efficient detection of NH<sub>3</sub> at room temperature. When exposed to 100 ppm ammonia, the sensor response reached 93%, with a response time of approximately 10 s, representing a tenfold improvement over bare MoO<sub>3</sub>. The surplus electrons on the Ti<sub>3</sub>C<sub>2</sub>T<sub>x</sub>-30 surface facilitate the generation of species, further enhancing the stability of the MXene surface. In the presence of adsorbed MoO<sub>3</sub>, these species actively react with ammonia molecules, leading to significant changes in system resistance. Consequently, by incorporating an optimally proportioned Ti<sub>3</sub>C<sub>2</sub>T<sub>x</sub>, a significant breakthrough has been achieved for metal oxides in realizing high gas sensitivity at room temperature.

Yang et al. introduced a novel sensor by integrating SnO<sub>2</sub> quantum dot (QD) nanoparticles with Ti<sub>3</sub>C<sub>2</sub>T<sub>x</sub> MXene, achieving a composite material that exhibits enhanced sensing capabilities (Yang et al., 2024). The successful fabrication of this composite was thoroughly characterized through transmission electron microscopy (TEM) imaging and elemental mapping analysis, as demonstrated in Figures 1M–O. This innovative approach not only highlights the synergistic effects of combining these two materials but also paves the way for advanced gas sensing applications with

TABLE 1 Summary of recent researches on Metal oxide composite  $Ti_3C_2T_x$  MXene sensors for gas detection.

Gas	Sensing material	Synthesis method	Concentration (ppm)	Temperature (°C)	Response	Selectivity	References
NH <sub>3</sub>	Pt-Ti <sub>3</sub> C <sub>2</sub> T <sub>x</sub> /TiO <sub>2</sub>	hydrothermal	100	room temperature	45.5%	NO <sub>2</sub> , H <sub>2</sub> S, C <sub>2</sub> H <sub>6</sub> O, C <sub>4</sub> H <sub>10</sub> O, C <sub>3</sub> H <sub>8</sub> O, C <sub>3</sub> H <sub>6</sub> O, CH <sub>4</sub> O, CH <sub>2</sub> O	Zhang et al. (2023)
	SnO <sub>2</sub> QDs/Ti <sub>3</sub> C <sub>2</sub> T <sub>x</sub>	water-dispersible	100	room temperature	10.4	C <sub>3</sub> H <sub>6</sub> O, C <sub>2</sub> H <sub>6</sub> O, Toluene, CH <sub>4</sub> O	Yang et al. (2024)
	Ti <sub>3</sub> C <sub>2</sub> T <sub>x</sub> /CeO <sub>2</sub> /TiO <sub>2</sub> yarns	hydrothermal	100	room temperature	42.9%	C <sub>3</sub> H <sub>7</sub> NO, CH <sub>3</sub> COOH, H <sub>2</sub> S, HCHO, C <sub>2</sub> H <sub>5</sub> OH	Zhao et al. (2024b)
	BaTiO <sub>3</sub> /Ti <sub>3</sub> C <sub>2</sub> T <sub>x</sub>	hydrothermal	20	room temperature	10.43	C <sub>2</sub> H <sub>6</sub> O, CO, SO <sub>2</sub> , H <sub>2</sub> S, C <sub>6</sub> H <sub>6</sub>	Sun et al. (2024)
	Ti <sub>3</sub> C <sub>2</sub> T <sub>x</sub> /SnO <sub>2</sub>	hydrothermal	500	room temperature	75%	C <sub>2</sub> H <sub>6</sub> OH, H <sub>2</sub> , CH <sub>4</sub> , H <sub>2</sub> S, C <sub>3</sub> H <sub>6</sub> O	Yu et al. (2023)
NO <sub>2</sub>	Ti <sub>3</sub> C <sub>2</sub> T <sub>x</sub> /ZnO nanorod hybrids	hydrothermal	0.2	room temperature	346%	SO <sub>2</sub> , NH <sub>3</sub> , H <sub>2</sub> S, CO	Wang et al. (2022)
	In <sub>2</sub> O <sub>3</sub> /Ti <sub>3</sub> C <sub>2</sub> T <sub>x</sub>	hydrothermal	0.25	room temperature	193.45%	NO, CO <sub>2</sub> , NH <sub>3</sub> , CH <sub>4</sub> , H <sub>2</sub>	Fan et al. (2024)
	SnO <sub>2</sub> nanoparticles@Ti <sub>3</sub> C <sub>2</sub> T <sub>x</sub>	one-step solvothermal	300	room temperature	78.2%	CO, H <sub>2</sub> , NO <sub>2</sub> , H <sub>2</sub> S, NH <sub>3</sub>	Liu et al. (2024)
	few-layered Ti <sub>3</sub> C <sub>2</sub> T <sub>x</sub> /WO <sub>3</sub>	electrostatic self-assembly	20	200	89.46	NH <sub>3</sub> , CO, C <sub>6</sub> H <sub>6</sub> , C <sub>3</sub> H <sub>6</sub> O, Xylene, Toluene, CH <sub>4</sub> O, CH <sub>2</sub> O, C <sub>2</sub> H <sub>6</sub> O	Gao et al. (2023)
	Ti <sub>3</sub> C <sub>2</sub> T <sub>x</sub> /ZnO	electrostatic self-assembly, hydrothermal	50	80	190%	NH <sub>3</sub> , C <sub>3</sub> H <sub>6</sub> O, C <sub>7</sub> H <sub>8</sub> , CH <sub>3</sub> OH, CH <sub>2</sub> O, C <sub>3</sub> H <sub>8</sub> O, C <sub>2</sub> H <sub>6</sub> O, CO	Liu et al. (2023)
C <sub>3</sub> H <sub>6</sub> O	alpha-Fe <sub>2</sub> O <sub>3</sub> /TiO <sub>2</sub> /Ti <sub>3</sub> C <sub>2</sub> T <sub>x</sub>	hydrothermal, annealing treatments	100	220	34.66	C <sub>2</sub> H <sub>6</sub> O, CH <sub>4</sub> O, CH <sub>2</sub> O, C <sub>7</sub> H <sub>8</sub>	Zhao et al. (2024c)
	alpha-gamma-Fe <sub>2</sub> O <sub>3</sub> /TiO <sub>2</sub> /Ti <sub>3</sub> C <sub>2</sub> T <sub>x</sub>	hydrothermal	100	240	105.5	C <sub>8</sub> H <sub>10</sub> , C <sub>2</sub> H <sub>6</sub> O, CH <sub>4</sub> O, CH <sub>2</sub> O, H <sub>2</sub> S, NO <sub>2</sub> , NH <sub>3</sub> , C <sub>2</sub> O	Huang et al. (2024b)
	TiO <sub>2</sub> /Fe <sub>2</sub> O <sub>3</sub> -Ti <sub>3</sub> C <sub>2</sub> T <sub>x</sub>	hydrothermal	100	268	446.8	C <sub>8</sub> H <sub>10</sub> , C <sub>2</sub> H <sub>6</sub> O, CH <sub>4</sub> O, CH <sub>2</sub> O, H <sub>2</sub> S, NO <sub>2</sub> , NH <sub>3</sub> , CO	Huang et al. (2023)
	Ti <sub>3</sub> C <sub>2</sub> T <sub>x</sub> /rGO/CuO	hydrothermal	100	Room Temperature	52.9%	C <sub>6</sub> H <sub>6</sub> , N(CH <sub>3</sub> ) <sub>3</sub> , CH <sub>4</sub> O, C <sub>7</sub> H <sub>8</sub> , (C <sub>2</sub> H <sub>5</sub> ) <sub>3</sub> N	Liu et al. (2021)
(C <sub>2</sub> H <sub>5</sub> ) <sub>3</sub> N	In <sub>2</sub> O <sub>3</sub> nanofibers/Ti <sub>3</sub> C <sub>2</sub> T <sub>x</sub>	electrospinning	50	120	12.44	CH <sub>2</sub> O, C <sub>2</sub> H <sub>6</sub> O, C <sub>3</sub> H <sub>6</sub> O, CH <sub>4</sub> O, NH <sub>3</sub> , C <sub>6</sub> H <sub>6</sub>	Xie et al. (2024)
	Cr <sub>2</sub> O <sub>3</sub> /TiO <sub>2</sub> /Ti <sub>3</sub> C <sub>2</sub> T <sub>x</sub>	hydrothermal	5	Room Temperature	28%	NH <sub>3</sub> , C <sub>2</sub> H <sub>6</sub> O, C <sub>3</sub> H <sub>8</sub> O, C <sub>3</sub> H <sub>6</sub> O, C <sub>7</sub> H <sub>8</sub> , N(CH <sub>3</sub> ) <sub>3</sub> , CH <sub>4</sub> O, CO, NO <sub>2</sub>	Yao et al. (2023a)
CH <sub>2</sub> O	Ti <sub>3</sub> C <sub>2</sub> T <sub>x</sub> /SnO <sub>2</sub>	hydrothermal, freeze-dry	10	room temperature	29.16%	C <sub>2</sub> H <sub>6</sub> O, C <sub>3</sub> H <sub>6</sub> O, N(CH <sub>3</sub> ) <sub>3</sub> , CH <sub>4</sub> O, NH <sub>3</sub>	Zhang et al. (2024a)
	ZnSnO <sub>3</sub> nanocubes/Ti <sub>3</sub> C <sub>2</sub> T <sub>x</sub>	hydrothermal	5	room temperature	62.4%	NH <sub>3</sub> , C <sub>2</sub> H <sub>6</sub> O, C <sub>6</sub> H <sub>6</sub> , C <sub>3</sub> H <sub>6</sub> O, N(CH <sub>3</sub> ) <sub>3</sub>	Sima et al. (2022)
C <sub>2</sub> H <sub>6</sub> O	ZnO/Ti <sub>3</sub> C <sub>2</sub> T <sub>x</sub>	hydrothermal	100	300	79	C <sub>3</sub> H <sub>6</sub> O, CH <sub>4</sub> O, C <sub>3</sub> H <sub>8</sub> O, NH <sub>3</sub>	Bu et al. (2023)
	MoO <sub>2</sub> /MoO <sub>3</sub> /Ti <sub>3</sub> C <sub>2</sub> T <sub>x</sub>	hydrothermal	200	room temperature	19.77	N(CH <sub>3</sub> ) <sub>3</sub> , C <sub>3</sub> H <sub>6</sub> O, CH <sub>4</sub> O, CH <sub>2</sub> O, (C <sub>2</sub> H <sub>5</sub> ) <sub>3</sub> N	Zhang et al. (2022)

improved sensitivity and selectivity. The abundant nucleation sites on the MXene surface facilitated the dense deposition of SnO<sub>2</sub> QD nanoparticles with diameters ranging from 2 to 3 nm. Compared to traditional methods, SnO<sub>2</sub>-composited Ti<sub>3</sub>C<sub>2</sub>T<sub>x</sub> MXene materials

markedly improve the detection performance for NH<sub>3</sub> at room temperature, exhibiting a response that is 100 times greater than that of intrinsic Ti<sub>3</sub>C<sub>2</sub>T<sub>x</sub> MXene materials. These findings provide new insights into the development of gas sensors and signify the

potential applications of MXene-based materials in environmental monitoring.

Peng et al. successfully synthesized transition metal oxide-derived copper oxide (CuO) nanoparticles (NPs) through a hydrothermal method combined with stirring aging techniques (Peng et al., 2024). The resultant CuO NPs exhibited octahedral growth on the surface of  $Ti_3C_2T_x$  MXene nanosheets. The successful fabrication of this composite material was substantiated by X-ray diffraction (XRD) analysis, which revealed distinct crystallographic peaks corresponding to the synthesized phases, as illustrated in Figure 1P. This innovative approach signifies a notable advancement in the integration of metal oxides with MXene substrates, paving the way for enhanced functionalities in various applications. The resulting binary heterostructure, CuO NPs/ $Ti_3C_2T_x$  MXene, retains the unique structure of the metal-organic framework (MOF), featuring abundant heterojunction interfaces.  $Ti_3C_2T_x$  MXene materials compounded with CuO nanoparticles exhibit the unique structure of metal-organic frameworks (MOFs), and the characteristics associated with MOFs result in a larger specific surface area, abundant active sites, and a more intricate porous structure, thereby significantly enhancing their adsorption performance for  $NO_2$ . Under room temperature conditions, the sensor exhibits a sensitive response time of 38.54 s–100 ppm  $NO_2$ , with a total response time of 2.84 s. Furthermore, the detection limit for  $NO_2$  is as low as 30 ppb, maintaining good stability over a testing period of 10 weeks. This research positions the composite sensor as a high-sensitivity tool for  $NO_2$  monitoring, showcasing significant potential for applications at room temperature.

Xiong et al. developed a flexible ammonia sensor utilizing a composite material comprising polyaniline (PANI),  $Ti_3C_2T_x$ , and  $TiO_2$  through ultrasonic spray pyrolysis and *in situ* polymerization techniques (Xiong et al., 2023). The successful synthesis of this composite was characterized by X-ray diffraction (XRD) and Raman spectroscopy, as shown in Figures 1Q, R. This innovative methodology not only enhances the sensor's performance but also exemplifies the potential for integrating advanced materials to facilitate heightened sensitivity and responsiveness in gas detection applications. The synthesized  $TiO_2$  nanoparticles are uniformly adhered to the surface of  $Ti_3C_2T_x$ , effectively preventing aggregation in the PMT. Leveraging this characteristic, the enhanced PMT film sensor demonstrates high response (2.30), low detection limit (20 ppb), and high selectivity for 10 ppm  $NH_3$  at room temperature. Currently, considerable attention is being devoted to the incorporation of metal oxides into  $Ti_3C_2T_x$  MXene materials to form heterojunction structures. In addition to the aforementioned typical metal oxide- $Ti_3C_2T_x$  heterojunctions, we provide an overview of representative studies on metal oxide- $Ti_3C_2T_x$  heterojunctions for greenhouse gas detection, focusing primarily on  $NO_2$  and  $NH_3$  detection, which are summarized in Table 1.

### 2.3 Alternative materials composite $Ti_3C_2T_x$ MXene nanomaterials

Kim et al. successfully prepared three-dimensional  $MoS_2$ /MXene van der Waals heterostructure aerogels through the physical mixing of two-dimensional MXene and  $MoS_2$ , followed

by a freeze-drying method (Kim et al., 2023). This low-temperature synthesis approach effectively mitigated the significant oxidation of  $Ti_3C_2T_x$  MXene while forming a layered, independent three-dimensional heterostructure composed of high-quality  $MoS_2$  and MXene nanosheets. The catalytic layer of  $MoS_2$  significantly enhanced the functionalization of MXene, improving its sensitivity and long-term stability towards  $NO_2$  gas. Additionally, a resistive sensor based on  $WS_2$ / $Ti_3C_2T_x$  MXene multilayer composites was designed by Sardana et al. (Sardana et al., 2023). The optimal concentration ratio of a chemical resistive sensor was explored by combining different concentrations of  $WS_2$  with MXene. Notably, the composite  $Ti_3C_2T_x$  MXene sensor containing 25 wt%  $WS_2$  exhibited responses of 29% to 5 ppm  $NH_3$  and 44% to 100 ppb  $NO_2$  at room temperature, along with strong selectivity.

To achieve low detection limits and high sensitivity for  $NH_3$  detection at room temperature, a gas sensor based on a polypyrrole (PPy) coated MXene/ $MoS_2$  nanocomposite has been developed by Lu et al. (Lu L. et al., 2023). This loosely assembled heterogeneous structure of MXene-loaded  $MoS_2$  was synthesized through a one-step hydrothermal technique based on electrostatic self-assembly. The  $MoS_2$  nanosheets uniformly wrapped around the etched MXene surface formed a highly synergistic metal-semiconductor contact, effectively generating a resistive layer capable of capturing electrons produced during  $NH_3$  sensing. PPy was subsequently coated onto the MXene/ $MoS_2$  composite surface via an *in situ* polymerization process, resulting in a self-supporting structure. The  $Ti_3C_2T_x$  MXene/ $MoS_2$ /PPy composite material exhibits a high response to 100 ppm  $NH_3$  that is five times greater than that of intrinsic  $Ti_3C_2T_x$  MXene materials, while maintaining a response of 2.08 for 10 ppm  $NH_3$  at room temperature. The MXene/ $MoS_2$ /PPy nanocomposite sensor also displayed excellent long-term stability, high response and recovery rates, outstanding humidity resistance, and notable selectivity towards  $NH_3$ .

A shell-type  $Ti_3C_2T_x$ @PDAC (croconaine) composite material was designed by Zhou et al. through a simple *in situ* polymerization reaction for the detection of  $NH_3$  at room temperature (Zhou et al., 2023). Compared to the original  $Ti_3C_2T_x$  sensors constructed from the  $Ti_3C_2T_x$ -PDAC composite exhibited remarkable sensitivity, achieving a response of 2.8%  $ppm^{-1}$  with an estimated detection limit of 50 ppb. Under room temperature conditions, the  $Ti_3C_2T_x$ -PDAC sensor demonstrated commendable stability and durability, maintaining effective responsiveness to both 10 ppm and 500 ppb  $NH_3$  over a period of 45 days. Concurrently, Quan et al. devised a fully flexible paper-based gas sensor that integrated non-metallic  $Ti_3C_2T_x$  MXene electrodes with a  $Ti_3C_2T_x$ / $WS_2$  sensing film, forming ohmic contacts and Schottky heterojunctions within a single gas sensing channel (Quan et al., 2023). This  $Ti_3C_2T_x$ / $WS_2$  composite demonstrated high conductivity, effective charge transfer capabilities, and abundant gas-sensing active sites. Under room temperature conditions, this gas sensor achieved a response of 15.2% to 1 ppm  $NO_2$ , which is 3.2 times greater than that of an Au fingertip electrode integrated with a  $Ti_3C_2T_x$ / $WS_2$  sensor (4.8%) and 76.0 times greater than that of a MXene electrode integrated with a  $Ti_3C_2T_x$  sensor (0.2%). Furthermore, the design operated effectively at a detection limit of 11.0 ppb for  $NO_2$  gas

while exhibiting outstanding stability in high-humidity environments.

A film-type sensor based on a hybrid polyaniline (PANI:PSS) was developed by Wen et al. using a unique *in situ* polymerization technique (Wen et al., 2023). This sensor exhibits high sensitivity for NH<sub>3</sub> detection, yielding a favorable response to 1 ppm NH<sub>3</sub>. In terms of long-term stability and durability under greenhouse conditions, the PANI:PSS/Ti<sub>3</sub>C<sub>2</sub>T<sub>x</sub> sensor exhibited a mere 23% decrease in responsiveness to 1 ppm NH<sub>3</sub> after 30 consecutive hours of operation at room temperature. This result underscores the sensor's commendable stability, highlighting its potential for reliable application in extended environmental monitoring scenarios. Furthermore, it demonstrates notable selectivity, stability, and mechanical properties at room temperature. Additionally, a novel MoS<sub>2</sub>/Ti<sub>3</sub>C<sub>2</sub>T<sub>x</sub> heterostructure sensor was designed by Ta et al. using a hydrothermal method (Ta et al., 2022). Compared to traditional heterojunction sensors, the incorporation of two-dimensional metal sulfide MoS<sub>2</sub> with Ti<sub>3</sub>C<sub>2</sub>T<sub>x</sub> MXene significantly enhances the sensing performance, while the compatibility between MoS<sub>2</sub> and Ti<sub>3</sub>C<sub>2</sub>T<sub>x</sub> ensures stable sensing capabilities for NO<sub>2</sub> at room temperature. Building upon the work of Ta's team, Tian et al. incorporated a TiO<sub>2</sub> system into MoS<sub>2</sub>/Ti<sub>3</sub>C<sub>2</sub>T<sub>x</sub> materials to enhance the capacity for electron supply in the sensing material (Tian et al., 2022). Gas sensing tests revealed that, compared to intrinsic Ti<sub>3</sub>C<sub>2</sub>T<sub>x</sub> MXene and MoS<sub>2</sub> materials, the sensing performance of this composite material improved by 1.79 times and 2.75 times, respectively, for 100 ppm NH<sub>3</sub> at room temperature, while also exhibiting a lower detection limit. The Ti<sub>3</sub>C<sub>2</sub>T<sub>x</sub> MXene@TiO<sub>2</sub>/MoS<sub>2</sub> sensor demonstrated exceptional responsiveness to 100 ppm NH<sub>3</sub> at room temperature over a continuous monitoring period of 60 days, with a slight decrease in response of only 9.1%. The response value stabilized at approximately 163.3%, indicating the sensor's robust performance and potential for long-term applications in gas detection. These findings provide new perspectives for the development of gas sensors and illustrate the broad application potential of MXenes and their composites in environmental monitoring.

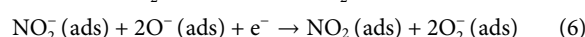
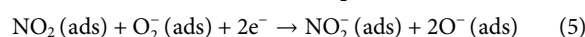
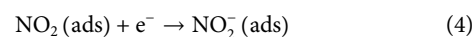
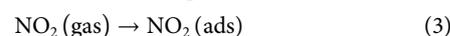
### 3 Sensing mechanisms of Ti<sub>3</sub>C<sub>2</sub>T<sub>x</sub> MXene heterojunction structures

Understanding the gas sensing mechanisms is crucial for the development of high-performance sensors based on Ti<sub>3</sub>C<sub>2</sub>T<sub>x</sub> MXene. The adsorbed gases can be primarily classified into oxidative and reductive gases. As shown in previous analyses, Ti<sub>3</sub>C<sub>2</sub>T<sub>x</sub> MXene exhibits exceptional responsiveness to toxic gases such as NO<sub>2</sub> and NH<sub>3</sub> commonly found in greenhouse environments (Jin et al., 2020; Seekaew et al., 2023; Cao et al., 2024). In this study, NO<sub>2</sub> is selected as a representative oxidative gas and NH<sub>3</sub> as a reductive gas for in-depth investigation. Research indicates that Ti<sub>3</sub>C<sub>2</sub>T<sub>x</sub> MXene, due to its high conductivity, large specific surface area, favorable hydrophilicity, and abundant surface functional groups, possesses excellent adsorption capabilities toward NO<sub>2</sub> (Nahirniak and Saruhan, 2022). Furthermore, existing studies have demonstrated that Ti<sub>3</sub>C<sub>2</sub>T<sub>x</sub> MXene materials can also respond favorably to the reductive gas NH<sub>3</sub> (Lee et al., 2017). Consequently, the traditional charge

transfer theories associated with metal oxides may not be applicable to the Ti<sub>3</sub>C<sub>2</sub>T<sub>x</sub> MXene materials.

### 3.1 Sensing mechanisms of Ti<sub>3</sub>C<sub>2</sub>T<sub>x</sub> MXene heterojunction structures for oxidative gases

During the composite process of Ti<sub>3</sub>C<sub>2</sub>T<sub>x</sub> MXene with In<sub>2</sub>O<sub>3</sub>, it has been observed that when NO<sub>2</sub> is adsorbed at room temperature, oxygen is initially adsorbed on the surface of In<sub>2</sub>O<sub>3</sub>, where it captures electrons to form superoxide anions O<sub>2</sub><sup>-</sup> (ads), as shown in Equations 1, 2 (Fan et al., 2024). Due to the greater electron affinity of NO<sub>2</sub> compared to that of O<sub>2</sub>, electrons on the surface of the sensing material are preferentially attracted to NO<sub>2</sub>, resulting in the formation of NO<sub>2</sub><sup>-</sup>. The specific process is illustrated in Equations 3–5. As electrons are continually captured from In<sub>2</sub>O<sub>3</sub> and flow towards Ti<sub>3</sub>C<sub>2</sub>T<sub>x</sub>, the Schottky barrier layer at the interface between Ti<sub>3</sub>C<sub>2</sub>T<sub>x</sub> and In<sub>2</sub>O<sub>3</sub> gradually expands. Upon expulsion of NO<sub>2</sub> gas from the chamber, the generated NO<sub>2</sub><sup>-</sup> reacts with O<sub>2</sub><sup>-</sup>, reverting back to NO<sub>2</sub>, as illustrated in Equation 6. In parallel, Guo et al. investigated the behavior of Ti<sub>3</sub>C<sub>2</sub>T<sub>x</sub>/CuO sensors when exposed to air (Guo et al., 2023). Research conducted by the team reveals that the sensing mechanism of the Ti<sub>3</sub>C<sub>2</sub>T<sub>x</sub>/CuO sensor involves the initial interaction of oxygen molecules in the air with the sensing layer, leading to the formation of adsorbed O<sub>2</sub> (ads). Subsequently, the adsorbed oxygen combines with captured electrons to form O<sub>2</sub><sup>-</sup> (ads). As illustrated in Figure 2A, oxygen vacancies within the Ti<sub>3</sub>C<sub>2</sub>T<sub>x</sub>/CuO nanocomposite also facilitate the conversion of O<sub>2</sub> (ads) into O<sub>2</sub><sup>-</sup> (ads). The depletion of electrons results in a continuous increase in hole concentration within CuO. Due to the work function difference between Ti<sub>3</sub>C<sub>2</sub>T<sub>x</sub> (3.9 eV) and CuO (4.7 eV), holes in CuO migrate towards Ti<sub>3</sub>C<sub>2</sub>T<sub>x</sub> while electrons from Ti<sub>3</sub>C<sub>2</sub>T<sub>x</sub> flow into CuO until the Fermi levels reach equilibrium. Throughout this process, the valence band thickens and the hole accumulation layer widens, resulting in an initial observation of reduced resistance in the Ti<sub>3</sub>C<sub>2</sub>T<sub>x</sub>/CuO sensor.



The MoS<sub>2</sub>/Ti<sub>3</sub>C<sub>2</sub>T<sub>x</sub> sensor developed by Ta captures O<sub>2</sub> molecules from the air at room temperature, resulting in the formation of superoxide anions as electrons are captured on the sensor surface (Ta et al., 2022). Moreover, the presence of TiO<sub>2</sub> facilitates the acquisition of additional oxygen ions by the sensor. As shown in Equation 7, due to its strong electron affinity and oxidative nature, NO<sub>2</sub> is capable of extracting electrons from the surrounding medium, resulting in electron depletion. The higher electronegativity of NO<sub>2</sub> compared to oxygen facilitates the reaction between NO<sub>2</sub> molecules and oxygen ions, leading to the formation of nitrate ions (NO<sub>3</sub><sup>-</sup>). Concurrently, the accumulation of holes promotes a reduction in resistance, inducing p-type semiconductor behavior. Notably, a

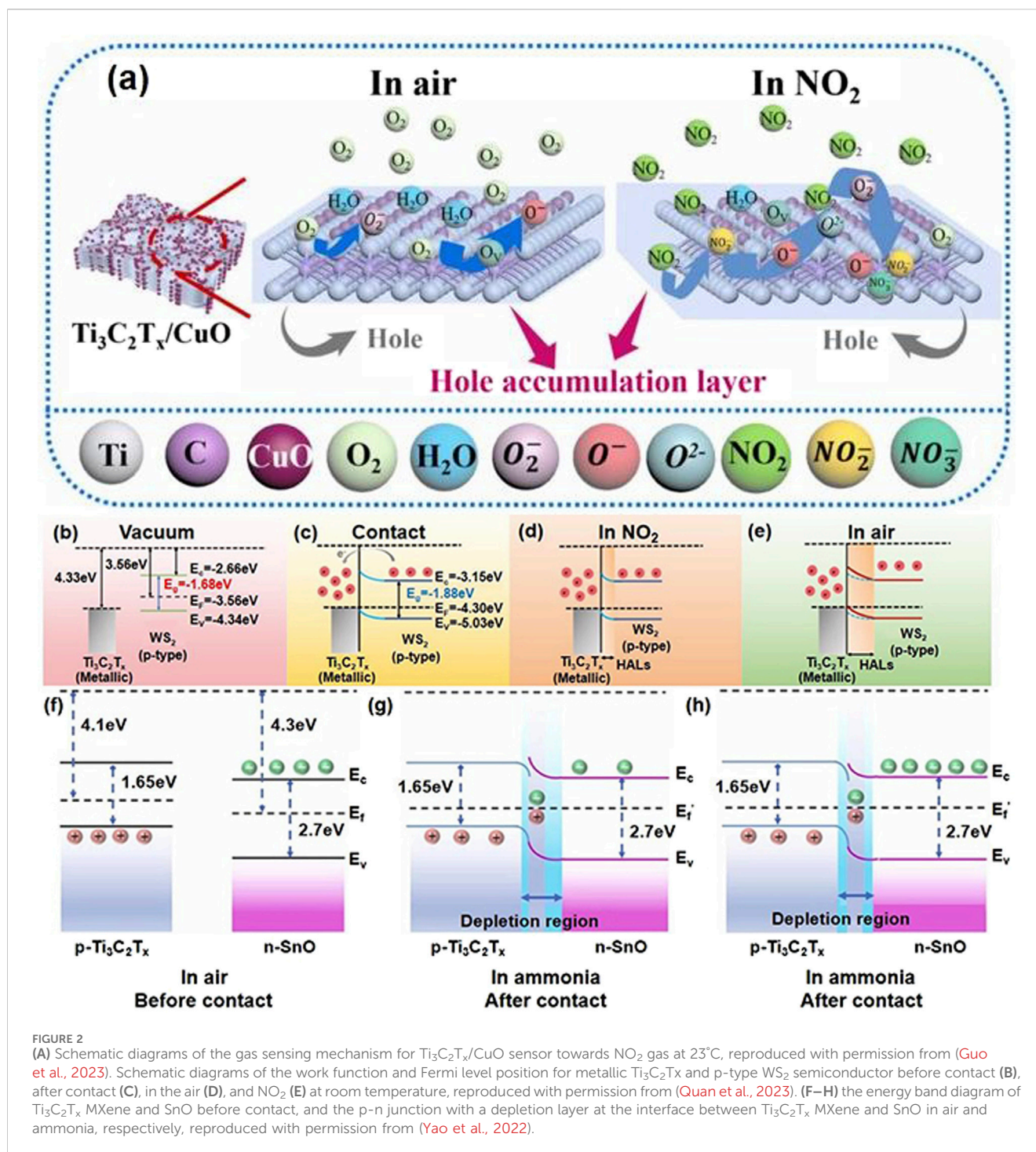


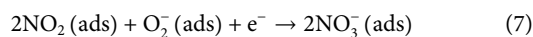
FIGURE 2

(A) Schematic diagrams of the gas sensing mechanism for  $\text{Ti}_3\text{C}_2\text{T}_x/\text{CuO}$  sensor towards  $\text{NO}_2$  gas at  $23^\circ\text{C}$ , reproduced with permission from (Guo et al., 2023). Schematic diagrams of the work function and Fermi level position for metallic  $\text{Ti}_3\text{C}_2\text{T}_x$  and p-type  $\text{WS}_2$  semiconductor before contact (B), after contact (C), in the air (D), and  $\text{NO}_2$  (E) at room temperature, reproduced with permission from (Quan et al., 2023). (F–H) the energy band diagram of  $\text{Ti}_3\text{C}_2\text{T}_x$  MXene and SnO before contact, and the p-n junction with a depletion layer at the interface between  $\text{Ti}_3\text{C}_2\text{T}_x$  MXene and SnO in air and ammonia, respectively, reproduced with permission from (Yao et al., 2022).

continuous heterojunction interface forms between vertically oriented  $\text{MoS}_2$  and layer-stacked  $\text{Ti}_3\text{C}_2\text{T}_x$  MXene, facilitating the accelerated migration of additional electrons. In this context, edges terminated with sulfur (S) and those terminated with molybdenum (Mo) exhibit high d-orbital electron densities, enhancing electronic interactions with  $\text{NO}_2$  gas. Furthermore, hydrogen bonding between  $\text{NO}_2$  molecules and water molecules under ambient humidity conditions also contributes to the adsorption of  $\text{NO}_2$ . In their investigation, Quan et al. similarly observed that when  $\text{Ti}_3\text{C}_2\text{T}_x/\text{WS}_2$  materials are exposed to

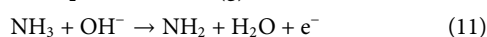
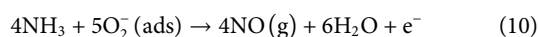
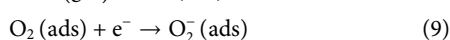
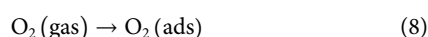
ambient air at room temperature, oxygen molecules can capture electrons from the material, resulting in the formation of chemically adsorbed oxide ions ( $\text{O}_2(\text{ads})$ ) on the surface (Quan et al., 2023). This interaction may lead to the establishment of a hole accumulation layer. Upon the introduction of  $\text{NO}_2$ , which possesses a higher electron affinity ( $2.30\text{ eV}$ ) compared to that of oxygen ( $0.44\text{ eV}$ ), electrons migrate toward the  $\text{NO}_2$ , facilitating the formation of nitrate ions ( $\text{NO}_3^-$ ). This process not only promotes electron extraction but also contributes to an increase in the hole accumulation layer,

ultimately resulting in a reduction in electrical resistance. The detailed reaction mechanism is illustrated in **Figures 2B–E**.



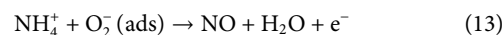
### 3.2 Sensing mechanisms of $\text{Ti}_3\text{C}_2\text{T}_x$ MXene heterojunction structures for reductive gases

It has been noted that in  $\text{TiO}_2/\text{Ti}_3\text{C}_2\text{T}_x$  MXene composites,  $\text{TiO}_2$ , as an n-type semiconductor with high electronegativity, may contain intrinsic oxygen vacancies and tends to adsorb oxygen from the atmosphere on its surface (Dogra et al., 2024). The adsorbed oxygen molecules capture electrons at the oxide surface, transforming into superoxide anions ( $\text{O}_2^-$ ), as represented in **Equations 8, 9**. It is important to acknowledge that competition for oxygen adsorption may occur between the semiconductor oxide and  $\text{Ti}_3\text{C}_2\text{T}_x$  within the composite. In any case, the adsorbed oxygen will convert to  $\text{O}_2^-$ . As an n-type semiconductor,  $\text{TiO}_2$  has a work function of 5.1 eV, while the typical range of the work function for  $\text{Ti}_3\text{C}_2\text{T}_x$  lies between 3.9 eV and 4.8 eV, depending on its surface terminating groups. Assuming a work function of 3.9 eV for MXene, electrons will flow from MXene to  $\text{TiO}_2$ , leading to the formation of a depletion layer at the  $\text{TiO}_2/\text{Ti}_3\text{C}_2\text{T}_x$  interface. When  $\text{NH}_3$  interacts with the sensing surface, it can contribute electrons through two different mechanisms, as illustrated in **Equations 10, 11**. On one hand,  $\text{NH}_3$  molecules may interact with the adsorbed  $\text{O}_2^-$  ions, releasing electrons in the process; on the other hand, gas molecules might also interact with  $\text{OH}^-$  ions, similarly resulting in electron release. The released electrons further compensate for the charge in the depletion layer, causing an increase in the sensor resistance.



Zhu et al. discovered that at room temperature (below 100 °C), oxygen adsorbed on the surface of  $\text{SnO}_2/\text{Ti}_3\text{C}_2\text{T}_x$  nanocomposites can ionize into superoxide anions ( $\text{O}_2^-$ ), as shown in **Equation 9** (Zhu et al., 2024). The entire reaction process can be described by **Equations 12, 13**. Yao et al. further investigated the behavior of  $\text{Ti}_3\text{C}_2\text{T}_x/\text{ZnO}$  when exposed to  $\text{NH}_3$  (Yao L. et al., 2023). Upon adsorption of  $\text{NH}_3$  molecules on the  $\text{Ti}_3\text{C}_2\text{T}_x/\text{ZnO}$  surface, a reaction occurs with water molecules to form ammonium ions ( $\text{NH}_4^+$ ). Subsequently, the interactions between the adsorbed  $\text{NH}_3$  and  $\text{NH}_4^+$  can also be articulated using **Equations 12, 13**. The electrons released from these reactions flow back to the  $\text{Ti}_3\text{C}_2\text{T}_x/\text{ZnO}$  material, where they recombine with holes in  $\text{Ti}_3\text{C}_2\text{T}_x$  MXene, resulting in a reduction of hole carriers in  $\text{Ti}_3\text{C}_2\text{T}_x/\text{ZnO}$  and an increase in its resistance. Subsequently, Yao et al. delved into the adsorption mechanism of  $\text{NH}_3$  on  $\text{Ti}_3\text{C}_2\text{T}_x/\text{SnO}$  sensors and discovered that this mechanism aligns with **Equations 12, 13** (Yao et al., 2022). The presence of p-n junctions enables the

composite material to function as an electron acceptor, receiving electrons from the external environment. This interaction leads to a reduction in resistance during the  $\text{NH}_3$  adsorption process for  $\text{Ti}_3\text{C}_2\text{T}_x$  MXene/ $\text{SnO}$ , as depicted in detail in **Figures 2F–H**. This insightful analysis underscores how the existence of p-n junctions facilitates effective electron transfer within the compound, resulting in enhanced sensitivity to  $\text{NH}_3$ .



$\text{Ti}_3\text{C}_2\text{T}_x$  MXene exhibits high conductivity, a large specific surface area, favorable hydrophilicity, and abundant surface terminal groups, enabling effective gas adsorption. However, research on the formation of heterojunctions between  $\text{Ti}_3\text{C}_2\text{T}_x$  MXene and transition metal sulfides for the detection of oxidative and reductive gases remains insufficient. Given that  $\text{Ti}_3\text{C}_2\text{T}_x$  MXene demonstrates good adsorption capabilities for both types of gases, directly applying traditional p-type semiconductor theory to  $\text{Ti}_3\text{C}_2\text{T}_x$  MXene materials may not be entirely appropriate (Kim et al., 2018; Radhakrishnan and Rout, 2023). Therefore, it is essential to consider additional factors in the analysis of resistance changes. On one hand,  $\text{Ti}_3\text{C}_2\text{T}_x$  MXene materials do not conform to the conventional definition of semiconductors; their metallic sensing layers may continually hinder the effective transport of charge carriers (Kim et al., 2018). On the other hand, the interlayer spacing of  $\text{Ti}_3\text{C}_2\text{T}_x$  MXene could influence its tolerance, representing an intriguing direction for further exploration. Additionally, the surface functional groups of  $\text{Ti}_3\text{C}_2\text{T}_x$  MXene materials play a crucial role in the gas sensing mechanism. Hydrophilic groups such as  $-\text{OH}$  and  $=\text{O}$  can interact with n-type or p-type semiconductors to enhance the adsorption of gas molecules onto the sensing material. For instance, MXene terminated with oxygen is an ideal candidate for  $\text{NH}_3$  sensing due to its semiconductor-like electronic properties (Bhardwaj and Hazra, 2021). Conversely, research by Hu et al. indicates that MXene terminated with sulfur is optimal for nitrogen oxide gas sensors (Hu et al., 2022). This research direction provides a new perspective on the applications of  $\text{Ti}_3\text{C}_2\text{T}_x$  MXene in gas sensing and lays the groundwork for the optimization and design of related materials.

## 4 Conclusion

This review provides a concise overview of the current research landscape surrounding gas sensors based on  $\text{Ti}_3\text{C}_2\text{T}_x$  MXene heterojunction structures. Analytical results indicate that  $\text{Ti}_3\text{C}_2\text{T}_x$  MXene nanostructures exhibit exceptional gas-sensing performance in greenhouse environments, attributed to their high electrical conductivity, extensive specific surface area, excellent hydrophilicity, and abundant surface terminal groups. The formation of heterojunction structures through composite materials has emerged as an effective strategy for enhancing the performance of  $\text{Ti}_3\text{C}_2\text{T}_x$  MXene sensors. The incorporation of metal atom doping, metal oxides, and transition metal sulfides into  $\text{Ti}_3\text{C}_2\text{T}_x$  MXene significantly improves the gas-sensing characteristics. Consequently, the development of  $\text{Ti}_3\text{C}_2\text{T}_x$

MXene heterojunction-based gas sensors presents immense potential for achieving room-temperature operation, low detection limits, and high responsiveness, particularly for gas monitoring in agricultural greenhouses. However, existing studies predominantly focus on the long-term stability and durability of these sensors under actual greenhouse conditions, mainly concerning ammonia, while investigations regarding common nitrogen oxides and other agricultural waste products remain limited. Moreover, the duration of performance stability testing is often short; thus, future research should extend these analyses to ensure prolonged usability of the sensors within intelligent greenhouse environments. In summary, this review underscores the capabilities of  $Ti_3C_2T_x$  MXene heterojunction gas sensors for monitoring toxic gases in greenhouses, highlighting their primary advantage of enabling high-sensitivity detection and rapid recovery of hazardous gases at room temperature. Future endeavors could integrate the methodologies discussed herein with reported approaches facilitating room-temperature, low-power, and highly sensitive sensing techniques, paving the way for the development of online monitoring sensor arrays for toxic gases in intelligent greenhouse systems. Additionally, establishing a quantitative detection model for multi-component mixed gases using artificial intelligence algorithms may enable direct detection of various toxic gas components within agricultural greenhouse settings.

## Author contributions

HZ: Conceptualization, Investigation, Writing—original draft. HX: Data curation, Writing—original draft. WZ: Writing—review and editing. ZW: Writing—review and editing. QZ: Writing—review and editing.

## References

- Assimakopoulos, F., Vassilakis, C., Margaris, D., Kotis, K., and Spiliotopoulos, D. (2024). The implementation of “smart” technologies in the agricultural sector: a review. *Information* 15 (8), 466. doi:10.3390/info15080466
- Bhardwaj, R., and Hazra, A. (2021). MXene-based gas sensors. *J. Mater. Chem. C* 9 (44), 15735–15754. doi:10.1039/d1tc04085e
- Bu, X., Wu, Q., Yuan, Y., Wu, H., Liu, W., Li, X., et al. (2023). The highly sensitive ethanol sensor based on nanocomposites of ZnO *in situ* grown on 2D  $Ti_3C_2T_x$  nanosheet. *Nanotechnology* 34 (10), 105707. doi:10.1088/1361-6528/aca8b1
- Cao, L. C. T., Chen, P. S., Lin, Y. H., Nagao, Y., Boonruang, S., Jong, C.-A., et al. (2024).  $Ti_3C_2T_x/MoO_3$  composite as an ultrasensitive and selective sensing material for a room-temperature nitrogen dioxide sensor. *Appl. Surf. Sci.* 676, 161025. doi:10.1016/j.apsusc.2024.161025
- Chen, B., Feng, A., Liu, K., Wu, J., Yu, Y., and Song, L. (2021). High-performance capacitive deionization using 3D porous  $Ti_3C_2T_x$  with improved conductivity. *J. Electroanal. Chem.* 895, 115515. doi:10.1016/j.jelechem.2021.115515
- Chen, Q., Zhang, Y., Tang, M., Wang, Z., and Zhang, D. (2024). A fast response hydrogen sensor based on the heterojunction of MXene and  $SnO_2$  nanosheets for lithium-ion battery failure detection. *Sensors Actuators B-Chemical* 405, 135229. doi:10.1016/j.snb.2023.135229
- Dogra, N., Gasso, S., Sharma, A., Sharma, K. K., and Sharma, S. (2024).  $TiO_2$  decorated MXene nanosheets for high-performance ammonia gas sensing at room-temperature. *Surfaces Interfaces* 48, 104290. doi:10.1016/j.surfin.2024.104290
- Fan, C., Yang, J., Mehrez, J.A.-A., Zhang, Y., Quan, W., Wu, J., et al. (2024). Mesoporous and encapsulated  $In_2O_3/Ti_3C_2T_x$  Schottky heterojunctions for rapid and ppb-level  $NO_2$  detection at room temperature. *ACS Sensors* 9 (5), 2372–2382. doi:10.1021/acssensors.3c02466
- Gao, J., Du, Q., Chen, K., Hou, M., Wang, Z., Yi, J., et al. (2023). Synthesis of few-layered  $Ti_3C_2T_x/WO_3$  nanorods foam composite material for  $NO_2$  gas sensing at low temperature. *Ceram. Int.* 49 (18), 29962–29970. doi:10.1016/j.ceramint.2023.06.253
- Guo, F., Feng, C., Zhang, Z., Zhang, L., Xu, C., Zhang, C., et al. (2023). A room-temperature  $NO_2$  sensor based on  $Ti_3C_2T_x$  MXene modified with sphere-like CuO. *Sensors Actuators B-Chemical* 375, 132885. doi:10.1016/j.snb.2022.132885
- Hassan, M. U., Huang, G., Arif, M. S., Mubarak, M. S., Tang, H., Xu, H., et al. (2024). Can urea-coated fertilizers be an effective means of reducing greenhouse gas emissions and improving crop productivity? *J. Environ. Manag.* 367, 121927. doi:10.1016/j.jenvman.2024.121927
- Hu, C., Yu, X., Li, Y., Cheng, J., Li, Q., and Xiao, B. (2022). Bandgap engineering of strained S-terminated MXene and its promising application as  $NO_x$  gas sensor. *Appl. Surf. Sci.* 592, 153296. doi:10.1016/j.apsusc.2022.153296
- Huang, D., Li, H., Liu, W., Chen, Y., Wang, W., Tan, X., et al. (2023). Coupling interface design of metal oxide heterostructures derived from MXene@MOFs hybrids for high-sensitivity acetone sensor. *Sensors Actuators B-Chemical* 383, 133594. doi:10.1016/j.snb.2023.133594
- Huang, D., Li, H., Liu, W., Tan, X., Zhao, M., and Liu, G. (2024b). Engineering metal oxide heterostructures derived from MOFs/MXene hybrids as efficient acetone sensor. *J. Alloys Compd.* 985, 174114. doi:10.1016/j.jallcom.2024.174114
- Huang, W., Sun, X., Sun, H., Feng, Y., Gong, X., Ma, Y., et al. (2024a). Effects of biochar and wood vinegar co-application on composting ammonia and nitrous oxide losses and fertility. *Bioresour. Technol.* 412, 131388. doi:10.1016/j.biortech.2024.131388
- Jin, L., Wu, C., Wei, K., He, L., Gao, H., Zhang, H., et al. (2020). Polymeric  $Ti_3C_2T_x$  MXene composites for room temperature ammonia sensing. *ACS Appl. Nano Mater.* 3 (12), 12071–12079. doi:10.1021/acsnm.0c02577

## Funding

The author(s) declare that financial support was received for the research, authorship, and/or publication of this article. This work has been supported in part by the National Natural Science Foundation of China (Nos 52077177 and 51507144) and the Fundamental Research Funds for the Central Universities (No. XDJK 2019B021).

## Conflict of interest

The authors declare that the research was conducted in the absence of any commercial or financial relationships that could be construed as a potential conflict of interest.

The author(s) declared that they were an editorial board member of *Frontiers*, at the time of submission. This had no impact on the peer review process and the final decision.

## Generative AI statement

The author(s) declare that no Generative AI was used in the creation of this manuscript.

## Publisher's note

All claims expressed in this article are solely those of the authors and do not necessarily represent those of their affiliated organizations, or those of the publisher, the editors and the reviewers. Any product that may be evaluated in this article, or claim that may be made by its manufacturer, is not guaranteed or endorsed by the publisher.

- Kale, S., Sabale, D., Srivastava, R., Londhe, V. P., and Kale, S. N. (2024). A synergistic combination of 2D MXene and MoO<sub>3</sub> nanoparticles for improved gas sensing at room temperature. *J. Phys. D-Applied Phys.* 57 (32), 325101. doi:10.1088/1361-6463/ad436b
- Kim, S., Shin, H., Lee, J., Park, C., Ahn, Y., Cho, H.-J., et al. (2023). Three-dimensional MoS<sub>2</sub>/MXene heterostructure aerogel for chemical gas sensors with superior sensitivity and stability. *ACS Nano* 17 (19), 19387–19397. doi:10.1021/acsnano.3c07074
- Kim, S. J., Koh, H.-J., Ren, C. E., Kwon, O., Maleski, K., Cho, S.-Y., et al. (2018). Metallic Ti<sub>3</sub>C<sub>2</sub>T<sub>x</sub> MXene gas sensors with ultrahigh signal-to-noise ratio. *ACS Nano* 12 (2), 986–993. doi:10.1021/acsnano.7b07460
- Kormann, R., Paixao, C. A., Hungria, M., Nogueira, M. A., and da Cruz, S. P. (2024). An innovative prototype to measure carbon dioxide, ethylene, and nitric and nitrous oxides in the soil air. *Commun. Soil Sci. Plant Analysis* 55 (19), 2909–2922. doi:10.1080/00103624.2024.2378985
- Kwon, J., Ha, Y., Choi, S., Jung, D. G., An, H. K., Kong, S. H., et al. (2024). Solution-processed NO<sub>2</sub> gas sensor based on poly(3-hexylthiophene)-doped PbS quantum dots operable at room temperature. *Sci. Rep.* 14 (1), 20600. doi:10.1038/s41598-024-71453-9
- Lee, E., Mohammadi, A. V., Prorok, B. C., Yoon, Y. S., Beidaghi, M., and Kim, D.-J. (2017). Room temperature gas sensing of two-dimensional titanium carbide (MXene). *ACS Appl. Mater. Interfaces* 9 (42), 37184–37190. doi:10.1021/acsmi.7b11055
- Li, Q., Li, Y., and Zeng, W. (2021a). Preparation and application of 2D MXene-based gas sensors: a review. *Chemosensors* 9 (8), 225. doi:10.3390/chemosensors9080225
- Li, Q., Xu, M., Jiang, C., Song, S., Li, T., Sun, M., et al. (2023). Highly sensitive graphene-based ammonia sensor enhanced by electrophoretic deposition of MXene. *Carbon* 202, 561–570. doi:10.1016/j.carbon.2022.11.033
- Li, S., Yu, L., Zhang, Y., Zhang, C., Cao, L., Nan, N., et al. (2024). Fe<sub>2</sub>O<sub>3</sub> nanoplate/TiO<sub>2</sub> nanoparticles supported by 2D Ti<sub>3</sub>C<sub>2</sub>T<sub>x</sub> MXene conductive layers for sensitive detection of NH<sub>3</sub> at room temperature. *Sensors Actuators B-Chemical* 413, 135890. doi:10.1016/j.snb.2024.135890
- Li, W., Wang, F., Zhang, Z., and Min, S. (2021b). MAPbI<sub>3</sub> microcrystals integrated with Ti<sub>3</sub>C<sub>2</sub>T<sub>x</sub> MXene nanosheets for efficient visible-light photocatalytic H<sub>2</sub> evolution. *Chem. Commun.* 57 (63), 7774–7777. doi:10.1039/d1cc02511b
- Liu, M., Wang, Z., Song, P., Yang, Z., and Wang, Q. (2021). Flexible MXene/rGO/CuO hybrid aerogels for high performance acetone sensing at room temperature. *Sensors Actuators B-Chemical* 340, 129946. doi:10.1016/j.snb.2021.129946
- Liu, T., Jia, X., Qiao, L., Yang, J., Wang, S., Li, Y., et al. (2023). Conductometric NO<sub>2</sub> gas sensors achieved by design of Ti<sub>3</sub>C<sub>2</sub>T<sub>x</sub>@ZnO heterostructures for application around 80°C. *Sensors Actuators B-Chemical* 390, 133908. doi:10.1016/j.snb.2023.133908
- Liu, X., Zhang, H., Shen, T., and Sun, J. (2024). Flexible resistive NO<sub>2</sub> gas sensor of SnO<sub>2</sub>@Ti<sub>3</sub>C<sub>2</sub>T<sub>x</sub> MXene for room temperature application. *Ceram. Int.* 50 (1), 2459–2466. doi:10.1016/j.ceramint.2023.11.032
- Lu, D., Huang, L., Zhang, J., Zhang, Y., Feng, W., Zeng, W., et al. (2023a). Rh- and Ru-modified InSe monolayers for detection of NH<sub>3</sub>, NO<sub>2</sub>, and SO<sub>2</sub> in agricultural greenhouse: a dft study. *ACS Appl. Nano Mater.* 6 (15), 14447–14458. doi:10.1021/acsnano.3c02470
- Lu, L., Liu, M., Sui, Q., Zhang, C., Zou, Y., Xu, F., et al. (2023b). MXene/MoS<sub>2</sub> nanosheet/polypyrrole for high-sensitivity detection of ammonia gas at room temperature. *Mater. Today Commun.* 35, 106239. doi:10.1016/j.mtcomm.2023.106239
- Lu, L., Zhang, C., Zou, Y., Xu, F., Sun, L., and Xiang, C. (2024). Room-temperature humidity-resistant highly sensitive ammonia sensor based on a porous MXene/N<sub>2</sub>Ti<sub>3</sub>O<sub>7</sub> @polyaniline composite. *Sensors Actuators B-Chemical* 405, 135323. doi:10.1016/j.snb.2024.135323
- Nahiriak, S., and Saruhan, B. (2022). MXene heterostructures as perspective materials for gas sensing applications. *Sensors* 22 (3), 972. doi:10.3390/s22030972
- Nam, M. S., Kim, J.-Y., Mirzaei, A., Lee, M. H., Kim, H. W., and Kim, S. S. (2024). Au- and Pt-decorated Ti<sub>3</sub>C<sub>2</sub>T<sub>x</sub> MXenes for preparing self-heated and flexible NH<sub>3</sub> gas sensors. *Sensors Actuators B-Chemical* 403, 135112. doi:10.1016/j.snb.2023.135112
- Pang, J., Peng, S., Hou, C., Wang, X., Wang, T., Cao, Y., et al. (2023). Applications of MXenes in human-like sensors and actuators. *Nano Res.* 16 (4), 5767–5795. doi:10.1007/s12274-022-5272-8
- Peng, H., Yang, J., Lin, C., Qi, L., Li, L., and Shi, K. (2024). Gas-sensitive performance of metal-organic framework-derived CuO NPs/Ti<sub>3</sub>C<sub>2</sub>T<sub>x</sub> MXene heterostructures for efficient NO<sub>2</sub> detection at room temperature. *J. Alloys Compd.* 980, 173657. doi:10.1016/j.jallcom.2024.173657
- Qi, Z., Wang, S., Li, Y., Wang, L., Zhao, L., Ge, Q., et al. (2021). Scavenging activity and reaction mechanism of Ti<sub>3</sub>C<sub>2</sub>T<sub>x</sub> MXene as a novel free radical scavenger. *Ceram. Int.* 47 (12), 16555–16561. doi:10.1016/j.ceramint.2021.02.226
- Qin, W.-W., Hu, X.-F., Fan, J.-L., Liu, Y.-S., Tan, L.-P., Zhou, M., et al. (2023). One-step laser ablation of Fe clusters supported on Ti<sub>3</sub>C<sub>2</sub>T<sub>x</sub> nanosheets for enhanced NH<sub>3</sub> sensing at room temperature. *Ceram. Int.* 49 (11), 18353–18362. doi:10.1016/j.ceramint.2023.02.207
- Qiu, C., Zhang, H., Li, Q., Song, Y., An, F., Wang, H., et al. (2024). Controllable synthesis of 3D PdCu/Ti<sub>3</sub>C<sub>2</sub>T<sub>x</sub> hierarchical nanostructures for chemiresistive room temperature H<sub>2</sub> sensors. *Sensors Actuators B-Chemical* 417, 136215. doi:10.1016/j.snb.2024.136215
- Quan, W., Shi, J., Luo, H., Fan, C., Lv, W., Chen, X., et al. (2023). Fully flexible MXene-based gas sensor on paper for highly sensitive room-temperature nitrogen dioxide detection. *ACS Sensors* 8 (1), 103–113. doi:10.1021/acssensors.2c01748
- Radhakrishnan, S., and Rout, C. S. (2023). Recent developments in 2D MXene-based materials for next generation room temperature NO<sub>2</sub> gas sensors. *Nanoscale Adv.* 5 (18), 4649–4669. doi:10.1039/d3na00275f
- Sardana, S., Debnath, A. K., Aswal, D. K., and Mahajan, A. (2023). WS<sub>2</sub> nanosheets decorated multi-layered MXene based chemiresistive sensor for efficient detection and discrimination of NH<sub>3</sub> and NO<sub>2</sub>. *Sensors Actuators B-Chemical* 394, 134352. doi:10.1016/j.snb.2023.134352
- Seekaew, Y., Kamlue, S., and Wongchoosuk, C. (2023). Room-temperature ammonia gas sensor based on Ti<sub>3</sub>C<sub>2</sub>T<sub>x</sub> MXene/graphene oxide/CuO/ZnO nanocomposite. *ACS Appl. Nano Mater.* 6 (10), 9008–9020. doi:10.1021/acsnm.3c01637
- Simu, Z., Song, P., Ding, Y., Lu, Z., and Wang, Q. (2022). ZnSnO<sub>3</sub> nanocubes/Ti<sub>3</sub>C<sub>2</sub>T<sub>x</sub> MXene composites for enhanced formaldehyde gas sensing properties at room temperature. *Appl. Surf. Sci.* 598, 153861. doi:10.1016/j.apsusc.2022.153861
- Singh, N., Sharma, A. K., Sarkar, I., Prabhu, S., and Chadaga, K. (2024). IoT-based greenhouse technologies for enhanced crop production: a comprehensive study of monitoring, control, and communication techniques. *Syst. Sci. and Control Eng.* 12 (1), 2306825. doi:10.1080/21642583.2024.2306825
- Sun, G., Wang, C., Jia, J., Zhang, H., Hu, Y., Liu, Y., et al. (2024). High-performance ammonia detection of polymeric BaTiO<sub>3</sub>/Ti<sub>3</sub>C<sub>2</sub>T<sub>x</sub> MXene composite-based sensor for gas emission and leakage. *J. Electron. Mater.* 53 (7), 3426–3437. doi:10.1007/s11664-024-11146-1
- Ta, Q. T. H., Tri, N. N., and Noh, J.-S. (2022). Improved NO<sub>2</sub> gas sensing performance of 2D MoS<sub>2</sub>/Ti<sub>3</sub>C<sub>2</sub>T<sub>x</sub> MXene nanocomposite. *Appl. Surf. Sci.* 604, 154624. doi:10.1016/j.apsusc.2022.154624
- Tian, X., Yao, L., Cui, X., Zhao, R., Chen, T., Xiao, X., et al. (2022). A two-dimensional Ti<sub>3</sub>C<sub>2</sub>T<sub>x</sub> MXene@TiO<sub>2</sub>/MoS<sub>2</sub> heterostructure with excellent selectivity for the room temperature detection of ammonia. *J. Mater. Chem. A* 10 (10), 5505–5519. doi:10.1039/d1ta10773a
- Walubengo, D., Orina, I., Kubo, Y., and Owino, W. (2022). Physico-chemical and postharvest quality characteristics of intra and interspecific grafted tomato fruits. *J. Agric. Food Res.* 7, 100261. doi:10.1016/j.jafr.2021.100261
- Wang, B., Gao, X., He, J., Xiao, Y., Liu, Y., Jia, X., et al. (2024d). Room-temperature ppb-level NO<sub>2</sub> sensor based on three-dimensional Mo<sub>2</sub>CT<sub>x</sub> nano-crumpled spheres. *Sensors Actuators B-Chemical* 399, 134790. doi:10.1016/j.snb.2023.134790
- Wang, J., Yang, Y., and Xia, Y. (2022). Mesoporous MXene/ZnO nanorod hybrids of high surface area for UV-activated NO<sub>2</sub> gas sensing in ppb-level. *Sensors Actuators B-Chemical* 353, 131087. doi:10.1016/j.snb.2021.131087
- Wang, S., Jiang, Y., Liu, B., Duan, Z., Pan, H., Yuan, Z., et al. (2021). Ultrathin Nb<sub>2</sub>CT<sub>x</sub> nanosheets-supported polyaniline nanocomposite: enabling ultrasensitive NH<sub>3</sub> detection. *Sensors Actuators B-Chemical* 343, 130069. doi:10.1016/j.snb.2021.130069
- Wang, W., Yao, Y., Xin, J., Xie, L., Han, Y., and Zhu, Z. (2024c). Chemiresistive SnS<sub>2</sub>/Nb<sub>4</sub>C<sub>2</sub>T<sub>x</sub> gas sensor for detection triethylamine at room temperature. *Sensors Actuators B-Chemical* 407, 135437. doi:10.1016/j.snb.2024.135437
- Wang, X., Zhu, H., Shutes, B., Cui, H., Hou, S., and Yan, B. (2024a). Fertilization changes nitrogen and carbon concentrations in saline-alkali paddy soil and their relationship with gas emissions: an analysis from the perspective of functional genes. *Environ. Technol. and Innovation* 36, 103817. doi:10.1016/j.eti.2024.103817
- Wang, Y., Wang, Y., Jian, M., Jiang, Q., and Li, X. (2024b). MXene key composites: a new arena for gas sensors. *Nano-Micro Lett.* 16 (1), 209. doi:10.1007/s40820-024-01430-4
- Wen, X., Cai, Y., Nie, X., Xiong, J., Wang, Y., Song, H., et al. (2023). PSS-doped PANI nanoparticle/Ti<sub>3</sub>C<sub>2</sub>T<sub>x</sub> composites for conductometric flexible ammonia gas sensors operated at room temperature. *Sensors Actuators B-Chemical* 374, 132788. doi:10.1016/j.snb.2022.132788
- Xia, Q., Fan, Y., Li, S., Zhou, A., Shinde, N., and Mane, R. S. (2023). MXene-based chemical gas sensors: recent developments and challenges. *Diam. Relat. Mater.* 131, 109557. doi:10.1016/j.diamond.2022.109557
- Xie, Q., Ding, Y., Wang, Q., and Song, P. (2024). Fabrication of 1D/2D In<sub>2</sub>O<sub>3</sub> nanofibers/Ti<sub>3</sub>C<sub>2</sub>T<sub>x</sub> MXene composites for high performance detection of trimethylamine at low temperature. *Sensors Actuators B-Chemical* 405, 135338. doi:10.1016/j.snb.2024.135338
- Xiong, J., Cai, Y., Nie, X., Wang, Y., Song, H., Sharif, H. M. A., et al. (2023). PANI/3D crumpled Ti<sub>3</sub>C<sub>2</sub>T<sub>x</sub>/TiO<sub>2</sub> nanocomposites for flexible conductometric NH<sub>3</sub> sensors working at room temperature. *Sensors Actuators B-Chemical* 390, 133987. doi:10.1016/j.snb.2023.133987
- Xu, D., Ren, R., Zhao, H., and Zhang, S. (2024). Intelligent detection of muskmelon ripeness in greenhouse environment based on YOLO-RFEW. *Agronomy-Basel* 14 (6), 1091. doi:10.3390/agronomy14061091
- Yang, E., Park, K. H., Oh, T., and Kim, S. J. (2024). Ultra-dense SnO<sub>2</sub> QDs-decorated MXene nanosheets with high water dispersibility for rapid NH<sub>3</sub> sensing at room temperature. *Sensors Actuators B-Chemical* 409, 135542. doi:10.1016/j.snb.2024.135542

- Yao, L., Tian, X., Cui, X., Zhao, R., Chen, T., Xiao, X., et al. (2023b). Low operating temperature and highly selective  $\text{NH}_3$  chemiresistive gas sensors based on a novel 2D  $\text{Ti}_3\text{C}_2\text{T}_x/\text{ZnO}$  composite with p-n heterojunction. *Appl. Phys. Rev.* 10 (3), 031414. doi:10.1063/5.0138182
- Yao, L., Tian, X., Cui, X., Zhao, R., Xiao, M., Wang, B., et al. (2022). Two-dimensional  $\text{Ti}_3\text{C}_2\text{T}_x$  MXene/ $\text{SnO}$  nanocomposites: towards enhanced response and selective ammonia vapor sensor at room temperature. *Sensors Actuators B-Chemical* 358, 131501. doi:10.1016/j.snb.2022.131501
- Yao, Y., Wang, Z., Han, Y., Xie, L., Zhao, X., Shahrokhian, S., et al. (2023a). Conductometric  $\text{Cr}_2\text{O}_3/\text{TiO}_2/\text{Ti}_3\text{C}_2\text{T}_x$  gas sensor for detecting triethylamine at room temperature. *Sensors Actuators B-Chemical* 381, 133412. doi:10.1016/j.snb.2023.133412
- Yu, H., Dai, L., Liu, Y., Zhou, Y., Fan, P., Luo, J., et al. (2023).  $\text{Ti}_3\text{C}_2\text{T}_x$  MXene- $\text{SnO}_2$  nanocomposite for superior room temperature ammonia gas sensor. *J. Alloys Compd.* 962, 171170. doi:10.1016/j.jallcom.2023.171170
- Zhang, D., Jiang, J., Wang, T., Li, F., Yu, H., Dong, X., et al. (2024e). Flexible room temperature gas sensor based on  $\alpha\text{-Fe}_2\text{O}_3/\text{Ti}_3\text{C}_2\text{T}_x$  MXene composites for ppb-level  $\text{H}_2\text{S}$  detection. *Sensors Actuators B-Chemical* 421, 136543. doi:10.1016/j.snb.2024.136543
- Zhang, H., Wang, L., Zou, Y., Li, Y., Xuan, J., Wang, X., et al. (2023). Enhanced ammonia sensing response based on Pt-decorated  $\text{Ti}_3\text{C}_2\text{T}_x/\text{TiO}_2$  composite at room temperature. *Nanotechnology* 34 (20), 205501. doi:10.1088/1361-6528/acbbd2
- Zhang, J., Li, Z., Yang, H., Chen, W., Wang, Z., Zhou, H., et al. (2024c). Application of MXene composites for target gas detection in food safety. *Food Chem.* 460, 140620. doi:10.1016/j.foodchem.2024.140620
- Zhang, L., Kuang, Y., Dai, S., Wang, J., Zhao, J., and Song, Y. (2020). Kinetic enhancement of capturing and storing greenhouse gas and volatile organic compound: micro-mechanism and micro-structure of hydrate growth. *Chem. Eng. J.* 379, 122357. doi:10.1016/j.cej.2019.122357
- Zhang, S., Song, P., Zheng, Y., Ding, Y., and Wang, Q. (2022).  $\text{MoO}_2/\text{MoO}_3/\text{MXene}$  ternary nanocomposites for high-performance ethanol detection at room temperature. *J. Alloys Compd.* 925, 166663. doi:10.1016/j.jallcom.2022.166663
- Zhang, T., He, G., Gui, Y., Liu, S., Li, Y., and Cao, L. (2024b). Investigating the adsorption performance of agricultural greenhouses hazardous gases on Rh doped  $\text{HfX}_2$  (X=S, Se) monolayers through DFT for potential gas sensor applications. *Surfaces Interfaces* 52, 104914. doi:10.1016/j.surfin.2024.104914
- Zhang, Y., Li, Y., Jiang, Y., Duan, Z., Yuan, Z., Liu, B., et al. (2024d). Synergistic effect of charge transfer and interlayer swelling in  $\text{V}_2\text{CT}_x/\text{SnS}_2$  driving ultrafast and highly sensitive  $\text{NO}_2$  detection at room temperature. *Sensors Actuators B-Chemical* 411, 135788. doi:10.1016/j.snb.2024.135788
- Zhang, Y., Wang, M.-Y., San, X.-G., Shen, Y.-B., Wang, G.-S., Zhang, L., et al. (2024a).  $\text{Ti}_3\text{C}_2\text{T}_x/\text{SnO}_2$  P-N heterostructure construction boosts room-temperature detecting formaldehyde. *Rare Met.* 43 (1), 267–279. doi:10.1007/s12598-023-02456-0
- Zhao, H., He, X., Shi, Z., and Li, S. (2024a). Adsorption and sensing behavior of Cr-doped  $\text{WS}_2$  monolayer for hazardous gases in agricultural greenhouses: a DFT study. *Mater. Today Commun.* 40, 109405. doi:10.1016/j.mtcomm.2024.109405
- Zhao, Z., Lv, Z., Chen, Z., Zhou, B., and Shao, Z. (2024c).  $\alpha\text{-Fe}_2\text{O}_3/\text{TiO}_2/\text{Ti}_3\text{C}_2\text{T}_x$  nanocomposites for enhanced acetone gas sensors. *Sensors* 24 (8), 2604. doi:10.3390/s24082604
- Zhao, Z., Ma, S., Rahmatullah, A. B. M., Chen, Z., Pan, Y., Wu, L., et al. (2024b). Flexible gas-strain dual sensor based on PU-supported  $\text{Ti}_3\text{C}_2\text{T}_x/\text{CeO}_2/\text{TiO}_2$  yarns. *Mater. Sci. Semicond. Process.* 181, 108607. doi:10.1016/j.mssp.2024.108607
- Zhou, J., Shokouh, S. H. H., Cui, L., Jarvinen, T., Pitkanen, O., Lv, Z.-P., et al. (2023). An ultra-sensitive  $\text{NH}_3$  gas sensor enabled by an ion-in-conjugated polycroconaine/ $\text{Ti}_3\text{C}_2\text{T}_x$  core-shell composite. *Nanoscale Horizons* 8 (6), 794–802. doi:10.1039/d2nh00591c
- Zhu, X., Li, J., Chang, X., Gao, W., Chen, X., Niu, S., et al. (2024). Room temperature gas sensors for  $\text{NH}_3$  detection based on  $\text{SnO}_2$  films and lamellar-structured  $\text{Ti}_3\text{C}_2\text{T}_x$  MXene heterojunction nanocomposites. *Appl. Surf. Sci.* 660, 159976. doi:10.1016/j.apsusc.2024.159976